Plasma Effects on Resonant Phenomena

Anil Pradhan

Abstract:

The effect of autoionizing resonances in atomic systems and processes is reviewed. Theoretical framework for treating resonances in the coupled channel approximation using the R-matrix method, as well as approximations related to plasma applications are described. The former entails large-scale atomic computations, and the latter is based on a new method for including collisional, Stark, thermal and other broadening mechanisms. We focus particularly on the problem of opacities calculations in high-energy-density (HED) plasmas such as stellar interiors and inertial confinement fusion devices. The treatment is generally relevant to radiative and collisional processes as the cross sections become energy-temperature-density dependent. While the computational difficulty increases considerably, the reaction rates are significantly affected. The related issue of the Boltzmann-Saha equation-of-state and its variants in local-thermodynamic-equilibrium (LTE) is also explored as the intermediary between atomic data on the one hand and plasma environments on the other.

PACS: 32.80.-t; 32.80.Fb; 33.60.+q

1. Introduction

Resonant phenomena are ubiquitous in physics and stem from correlation effects. In AMO physics autoionizing resonances are due to electron correlation effects among bound and continuum states. They manifest themselves prominently in cross sections of various atomic and molecular processes in laboratory and astrophysical plasma sources. The shapes, magnitudes, and extent of resonances determines associated rates for spectral formation and experimental and observed spectra. The well-known Fano profile [1, 2, 3] is widely used to analyze isolated resonance structures, with parameters that may be compared with theoretical calculations.

On the other hand, overlapping infinite series of autoionizing resonances converging on to large numbers of excited levels are also of great importance. In general, they are not amenable to analytic formulation and require computationally intensive coupled channel calculations, the most powerful of which is the R-matrix method by P.G. Burke and collaborators [4].[1] Whereas the R-matrix method has long been utilized for a variety of atomic processes and applications, I focus on a large-scale application to plasma opacities that is of immense importance in astrophysics and nuclear fusion sources, but where R-matrix atomic calculations including resonant phenomena in an *ab initio* manner, and taking account of plasma effects, are exceedingly difficult [8, 9, 10, 11].

Opacity determines the light we see or detect. All radiation-matter interactions need to be considered in order to determine the opacity of a given plasma source or medium. Primary physical processes

[1] Following the original suggestion by U. Fano about the R-matrix theory of nuclear reactions by A.M. Lane and R.G. Thomas [5], P.G. Burke introduced it for atomic and molecular processes, as described in [4]. Later, M.J. Seaton and collaborators adapted the R-matrix method for large-scale calculations required for the Opacity Project [6].

Received . Accepted .

Anil Pradhan. Department of Astronomy, Chemical Physics Program, The Ohio State University, Columbus, OH 43210, USA

contributing to opacity are:

$$\kappa_{ijk}(\nu) = \sum_k A_k \sum_j F_j \sum_{i,i'} [\kappa_{bb(}(i,i';\nu) + \kappa_{bf}(i,\epsilon_{i'};\nu) + \kappa_{ff}(\epsilon_i,\epsilon''_i;\nu) + \kappa_{sc}(\nu)] \ . \quad (1)$$

The first two are the dominant processes; bb refers to bound-bound and bf to bound-free transitions or photoionization. The other two, free-free transitions and photon scattering, are generally much smaller and may be treated by simple approximations (viz. [6, 7]). In Eq. 1, A_k is the abundance of an element k, its ionization fraction F_j at a given temperature-density, i, i' are initial bound and final bound/continuum states, and ϵ represents the free electron energy.

2. Coupled channel R-matrix method and atomic-plasma effects

The state-of-the-art R-matrix (RM) method provides a powerful computational tool to implement the general coupled-channel theoretical framework. An atomic systems is represented by a N-electron core or target ion wavefunction χ_i coupled with an $(N+1)^{th}$ free electron wavefunction θ_i in a bound or continuum state of the (e + ion) system. The total (e + ion) wavefunction is then a quantum superposition expressed as

$$\Psi(E) = \mathcal{A} \sum_i (E_i)\chi_i\theta_i(k_i^2) + \sum_j c_j \Phi_j(E_j). \quad (2)$$

When the free electron kinetic energy $k_i^2 > 0$, the first sum on the RHS of Eq. 2 represents a coupled channel system for electron-ion scattering or half-scattering photoionization process [3]. Each channel is defined by the spin-orbital quantum symmetries $(S_iL_iJ_i)\ \ell_i s_i[SLJ]$. Rydberg series of resonances arise from photoexcitation of bound energy levels into (e + ion) continua comprising of coupled thresholds of the core ion. A particular type of resonances due to photoexcitation-of-core (PEC) or Seaton resonances are due to strong dipole transitions in the core ion where the continuum electron in a Rydberg level remain a 'spectator'. The Seaton PEC resonances constitute the detailed balance inverse of the dielectronic recombination process, wherein an (photo-)excited core ion undergoes radiative decay by emission of photons redward of the core transition wavelength. It is found that the huge Seaton resonances dominate the bound-free opacity in a plasma.

If the first summation on the RHS of Eq. 2 is neglected then the coupling effects in the (e + ion) wavefunction are excluded, yielding the distorted wave (DW) approximation that does not include autoionizing resonances in an *ab initio* manner as the RM method. Owing to its simplicity, the DW method has been employed in existing opacity models. While resonant phenomena are not included in the DW calculations, that contribution may be included perturbatively by considering autoionizing resonances on par with lines as bound-bound transitions and employing line broadening theory for plasma broadening. However, the detailed auotionization shapes over extended energy ranges and their precise effect on atomic rates is not taken into account in DW models.

The Opacity Project (OP [6]) was originally developed to implement the RM method but was computationally intractable for most complex atoms. In particular, it was found that inner-shell transitions from closed electronic shells into outer open subshells implies a large number of channels to be included in Eq. 2. In recent years, a renewed and extended version of OP has been initiated [14] and is now in progress for improved opacities with higher accuracy [8, 9, 10, 11].

For opacity calculations, the transition matrix elements are obtained with dipole operator $\mathbf{D} = \sum_i \mathbf{r}_i$, where the sum is over all electrons, which gives the generalized line strength as,

$$\mathbf{S} = \left| \left\langle \Psi_\mathbf{f} | \sum_{\mathbf{j=1}}^{\mathbf{N}} \mathbf{r_j} | \Psi_\mathbf{i} \right\rangle \right|^\mathbf{2} \quad (3)$$

The oscillator strength (f_{ij}), radiative decay rate (A_{ji}), photoionization cross section (σ_{PI}), and mass attenuation coefficient then can be expressed as follows

$$f_{ij} = \left[\frac{E_{ji}}{3g_i}\right] S, \;\; A_{ji}(sec^{-1}) = \left[0.8032 \times 10^{10} \frac{E_{ji}^3}{3g_j}\right] S, \; \sigma_{PI}(K\alpha, \nu) = \frac{4\pi^2 a_o^2 \alpha}{3} \frac{E_{ij}}{g_k} S \tag{4}$$

The Breit-Pauli R-matrix (BPRM) method incorporates relativistic effects using the Breit-Pauli (BP) Hamiltonian for the (e + ion) system in intermediate coupling, with a pair-coupling scheme $S_i L_l (J_i) l_i (K_i) s_i (SLJ\pi)$, whereby states $S_i L_i$ is split into fine-structure levels $S_i L_i J_i$, and $SLJ\pi$ is the total spin-orbital symmetry. Consequently, the number of channels becomes several times larger than the corresponding LS coupling case. A considerable body of work with the BPRM codes has been carried out under the follow-on project to OP, the Iron Project [15]. The IP work is based on BPRM codes and archived in the large amount of radiative and collisional data in databases NORAD [19] and OP/IP database Topbase [16].

3. Plasma environment and approximations

The practical limitation of the RM method for plasma applications is evident from Eq. 2. Computational constraints imply that only a finite and usually small number of excited core ion states and resulting channels may be explicitly included in the wavefunction expansion. This has implications in high-energy-density (HED) plasmas such as in stellar interiors or fusion devices, wherein a large number of excited states exist and differentially perturbed. The temperature regime may be in excess of $10^6 - 10^7$ K, with electron densities up to 10^{27} cm^{-3}. Among the largest R-matrix calculations carried out thus far are the recent ones for Fe ions Fe XVII , Fe XVIII and Fe XIX that constitute $\sim$85% of iron opacity at the boundary between the solar radiative and convection zones at radius $R_\odot$ = 0.713$\pm$0.001, where T=2 $\times$ 10^6K and electron density $N_e = 10^{23}$ cm^{-3} [8]. The number of core levels included in the R-matrix (e + ion) wavefunction expansion were 218 levels of Fe XVIII for the (e+Fe XVIII) $\rightarrow$ Fe XVII bound and continuum states, 276 levels of Fe XIX for the (e+Fe XIX) $\rightarrow$ Fe XVIII , and 99 LS terms of Fe XX for (e+Fe XX) $\rightarrow$ Fe XIX [9].

3.1. Equation-of-state

In addition to the theoretical limit of the RM method, an obvious limit is imposed by perturbations on atoms by the plasma environment depending on the specific temperature-density. That manifests itself via the equation-of-state that determines the atomic ionization state and level populations. The generally employed approximation is to assume local-thermodynamic-equilibrium (LTE), as defined by the Saha-Boltzmann equations. From an atomic-plasma physics point of view, a widely employed formulation (such as in OP) is the Mihalas-Hummer-Däppen (MHD) equation of state in the so-called "chemical picture"[13]. It is based on the concept of *occupational probability* w of an excited level being occupied at a given temperature and density such that the level population is

$$N_{ij} = \frac{N_j g_{ij} w_{ij} e^{-E_{ij}/kT}}{U_j}, \tag{5}$$

where w_{ij} are the occupation probabilities of levels i in ionization state j, and U_j is the atomic internal partition function. The occupation probabilities do not have a sharp cut-off, but approach zero for high-n as they are dissolved due to plasma interactions. The partition function is re-defined as

$$U_j = \sum_i g_{ij} w_{ij} e^{(-E_{ij}/kT)}. \tag{6}$$

E_{ij} is the excitation energy of level i, g_{ij} its statistical weight and T the temperature. The w_{ij} are obtained by free-energy minimization, and taking into account Stark ionization due to plasma

microfields [13]. Hence, the exact form of the equation-of-state numerically determines how many and how much the excited states of an atom contribute to opacity and radiation transport.

3.2. Broadening of autoionizing resonances

Unlike line broadening *intrinsic* autoionization (AI) decay rates are much larger relative to radiative rates. Therefore, one expects resonances to broaden, smear out, and dissolve into the continuum much more than lines when subjected to *extrinsic* HED plasma environments. Also, unlike line broadening for which theoretical formulations are well developed and long employed, there is no *ab initio* and general treatment for AI broadening. Even for line broadening the most elaborate methods are are precise only for hydrogenic and simple atomic systems and several approximations are necessary to apply those to complex atoms in realistic sources [6].

Recently, a general theoretical and computational formalism has been introduced for AI resonance broadening [10]. Analogous to line broadening, the physical mechanisms considered are: electron collisions (pressure broadening), ion microfields (Stark broadening), Doppler effect (thermal broadening), and free-free transitions. It has been shown that *extrinsic* plasma effects redistribute and shift resonance strengths, even as the broad *intrinsic* asymmetries of resonance profiles is discernible as in Fano profiles. Furthermore, while the shapes, magnitudes and extent of resonances is affected, the total integrated resonance oscillator strengths are conserved, independent of temperature and density. The energy-temperature-density dependent cross sections would elicit and introduce physical features in resonant processes in photoionization, (e + ion) excitation and recombination. The method should be generally applicable to atomic species in high-energy-density (HED) sources such as fusion plasmas and stellar interiors.

Whereas the main broadening mechanisms in AI broadening are physically similar to line broadening, their theoretical and computational treatment is quite different. Superimposed on intrinsic AI broadening in atomic cross sections the extent of resonances owing to extrinsic plasma effects renders much of the line broadening theory inapplicable, particularly for multi-electron systems. The *unbroadened* AI resonances themselves vary by orders of magnitude in width, shapes and heights, and incorporate two types: large features due to photoexcitation-of-core (PEC) below thresholds corresponding to dipole core transitions [12], and infinite Rydberg series of resonances converging on to each excited core level of the (e + ion) system. The generally employed Voigt line profiles obtained by convolution of a Lorentzian function for radiative and collisional broadening, and a Gaussian function for Doppler or thermal broadening, are found to be practically inapplicable for AI broadening. Numerically, the Voigt kernel is ill-conditioned since the collisional-to-Doppler width ratio Γ_c /Γ_d varies over a far wider range for resonances than lines and therefore unconstrained *a priori*.

The physical processes for broadening of AI resonances differ from lines qualitatively and quantitatively. However, line broadening processes and formulae may be generalized to develop a theoretical treatment and computational algorithm outlined herein (details to be presented elsewhere). The convolved bound-free photoionization cross section of level i may be written as:

$$\sigma_i(\omega) = \int \tilde{\sigma}(\omega')\phi(\omega', \omega)d\omega', \tag{7}$$

where σ and $\tilde{\sigma}$ are the cross sections with plasma-broadened and unbroadened AI resonance structures, ω is the photon energy (Rydberg atomic units are used throughout), and $\phi(\omega', \omega)$ is the normalized Lorentzian profile factor in terms of the *total* width Γ due to all AI broadening processes included:

$$\phi(\omega', \omega) = \frac{\Gamma(\omega)/\pi}{x^2 + \Gamma^2}, \tag{8}$$

where $x \equiv \omega - \omega'$. The crucial difference with line broadening is that AI resonances in the (e + ion) system correspond to and are due to quantum mechanical interference between discretized continua

defined by excited core ion levels in a multitude of channels. The coupled channel (CC) approximation, such as implemented by the R-matrix (RM) method (viz. [4, 6, 7]), accounts for AI resonances in an (e + ion) system with generally asymmetric profiles (unlike line profiles that are usually symmetric). Given N core ion levels corresponding to resonance structures,

$$\sigma(\omega) = \sum_i^N \left[\int \tilde{\sigma}(\omega') \left[\frac{\Gamma_i(\omega)/\pi}{x^2 + \Gamma_i^(\omega)} \right] d\omega' \right]. \tag{9}$$

With $x \equiv \omega' - \omega$, the summation is over all excited thresholds E_i included in the N-level CC or RM wavefunction expansion, and corresponding to total damping width Γ_i due to all broadening processes. The profile $\phi(\omega', \omega)$ is centered at each continuum energy ω, convolved over the variable ω' and relative to each excited core ion threshold i . In the present formulation we associate the energy to the effective quantum number relative to each threshold $\omega' \rightarrow \nu_i$ to write the total width as:

$$\begin{aligned} \Gamma_i(\omega, \nu, T, N_e) &= \Gamma_c(i, \nu, \nu_c) + \Gamma_s(\nu_i, \nu_s^*) \\ &+ \Gamma_d(A, \omega) + \Gamma_f(f - f; \nu_i, \nu_i'), \end{aligned} \tag{10}$$

pertaining to collisional Γ_c, Stark Γ_s, Doppler Γ_d, and free-free transition Γ_f widths respectively, with additional parameters as defined below. Without loss of generality we assume a Lorentizan profile factor that describes collisional-ion broadening which dominates in HED plasmas. We assume this approximation to be valid since collisional profile wings extend much wider as x^{-2}, compared to the shorter range $exp(-x^2)$ for thermal Doppler, and $x^{-5/2}$ for Stark broadening. In evaluating Eq. (10) from Eq. 9 the limits $\mp\infty$ are replaced by $\mp\Gamma_i/\sqrt{\delta}$; δ is chosen to ensure the Lorentzian profile energy range for accurate normalization (see Eq. 15). Convolution by evaluation of Eqs. (7,9) is carried out for each energy ω throughout the tabulated mesh of energies used to delineate all AI resonance structures, for each cross section, and each core ion threshold. We employ the following expressions for computations:

$$\Gamma_c(i, \nu) \; = \; 5 \left(\frac{\pi}{kT} \right)^{1/2} a_o^3 N_e G(T, z, \nu_i)(\nu_i^4/z^2), \tag{11}$$

where T, N_e , z, and A are the temperature, electron density, ion charge and atomic weight respectively, and ν_i is the effective quantum number relative to each core ion threshold i : $\omega \equiv E = E_i - \nu_i^2/z^2$ is a continuous variable. The Gaunt factor $G(T, z, \nu_i) = \sqrt{3}/\pi[1/2 + ln(\nu_i kT/z)]$. A factor $(n_x/n_g)^4$ is introduced for Γ_c to allow for doubly excited AI levels with excited core levels n_x relative to the ground configuration n_g (e.g. for Fe XVIII $n_x = 3, 4$ relative to the ground configuration $n_g = 2$). A treatment of the Stark effect for complex systems entails two approaches, one where both electron and ion perturbations are combined (viz. [18]), or separately (viz. [6, 10]) employed herein. Excited Rydberg levels are nearly hydrogenic and ion perturbations are the main broadening effect, though collisional broadening competes significantly increasing with density as well as ν_i^4 (Eq. 5). The total Stark width of a given n -complex is $\approx (3F/z)n^2$, where F is the plasma electric microfield. Assuming the dominant ion perturbers to be protons and density equal to electrons, N_e =N_p, we take $F = [(4/3)\pi a_o^3 N_e)]^{2/3}$, as employed in the Mihalas-Hummer-Däppen equation-of-state formulation [13].

$$\Gamma_s(\nu_i, \nu_s^*) = [(4/3)\pi a_o^3 N_e]^{2/3} \nu_i^2. \tag{12}$$

In addition, in employing Eq. (6) a Stark ionization parameter $\nu_s^* \; = \; 1.2 \times 10^3 N_e^{-2/15} z^{3/5}$ is introduced such that AI resonances may be considered fully dissolved into the continuum for $\nu_i > \nu_s^*$

(analogous to the Inglis-Teller series limit [17, 13]). Calculations are carried out with and without ν_s^* as shown later in Table 1. The Doppler width is:

$$\Gamma_d(A,T,\omega) = 4.2858 \times 10^{-7}\sqrt{(T/A)}, \tag{13}$$

where ω is *not* the usual line center but taken to be each AI resonance energy. The last term Γ_f in Eq. (5) accounts for free-free transitions among autoionizing levels with ν_i, ν_i' such that

$$X_i + e(E_i,\nu_i) \longrightarrow X_i' + e'(E_i',\nu_i'). \tag{14}$$

The large number of free-free transition probabilities for $+ve$ energy AI levels $E_i, E_i' > 0$ may be computed using RM or atomic structure codes.

Whereas Eq.9 has an analytical solution in terms of $tan^{-1}(x/\Gamma)/\Gamma$ evaluated at limiting values of $x \rightarrow \mp\Gamma/\sqrt{\delta}$, its evaluation for practical applications entails piece-wise integration across multiple energy ranges spanning many excited thresholds and different boundary conditions. For example, the total width Γ is very large at high densities and the Lorentzian profile may be incomplete above the ionization threshold and therefore not properly normalized. We obtain the necessary redward left-wing correction for partial re-normalization as

$$\lim_{a\rightarrow -\Gamma/2\sqrt{\delta}} \int_a^{+\Gamma/\sqrt{\delta}} \phi(\omega,\omega')d\omega' = \left[\frac{1}{4} - \frac{tan^{-1}(\frac{a}{\Gamma/2\sqrt{\delta}})}{\pi}\right], \tag{15}$$

where a is the lower energy range up to the ionization threshold, reaching the maximum value $-\Gamma/2\sqrt{\delta}$.

4. Results and discussion

All atomic cross sections with resonant phenomena are modified by the plasma environment. An exemplar from large-scale opacity calculations [8, 9, 10, 11] is presented in Fig. 1. The complexity and magnitude of computations is demonstrated for the (e + Fe XIX) $\longrightarrow$ Fe XVIII system in an highly excited level $2s^2 2p^4\ [^3P_0^e]\ 5s(^2P_{1/2})$ with ionization energy = 13.79 Ry, compared to the ground level $2s^2 2p^5\ ^2P_{1/2}^o$) = 98.9 Ry. We utilize new results from an extensive BPRM calculation with 276-levels dominated by $n = 2, 3, 4$ levels of the core ion Fe XIX [9], resulting in 1,601 bound levels of Fe XVIII with configurations up to $n \leq 10,\ \ell \leq 9,\ J \leq 12$). Rydberg series of AI resonances correspond to $(S_i L_i J_i)\ n\ell,\ n \leq 10, \ell \leq 9$, with effective quantum number defined as a continuous variable $\nu_i = z/\sqrt{(E_i - E)}\ (E > 0)$, up to the highest 276^{th} Fe XIX core level. AI resonances are resolved for all cross sections at ∼45,000 photon energies [9, 11].

Fig. 1 displays detailed results for plasma broadened and unbroadened photoionization cross section of one particular excited level $2s^2 2p^5[^2P_{3/2}^o]4d(^1F_3^o)$ (ionization energy = 17.626 Ry) of Fe XVII at four densities. The main features are as follows: (I) orders of magnitude variation in resonance heights and extent. (II) For $N_e > 10^{20}$/cc AI resonances begin to exhibit broadening and smearing of overlapping Rydberg series. $N_e = 10^{21}$cc. The narrower high-$n\ l$ resonances dissolve into the continua but stronger low-$n\ l$ resonance retain their characteristic asymmetric shapes. With increasing density $N_e = 10^{21-23}$cc, resonance structures not only broaden but their strengths shift and redistributed over a wide range determined by the total width $\Gamma(\omega, \nu_i, T, N_e)$ at each photon energy $\hbar\omega$ (Eq. 9). (III) The averaged step-wise structure due to Stark ionization cut-off (Table 1) represents complete dissolution into continua. (IV) It is numerically ascertained that total AI resonance strengths are conserved, and integrated values generally do not deviate by more than 1-2%. This is also an important accuracy check on numerical integration and the computational algorithm, as well as the choice of the parameter δ that determines the energy range of the Lorentizan profile at each T and N_e. In the present δ = 0.01 for all N_e =10^{20-23}/cc.

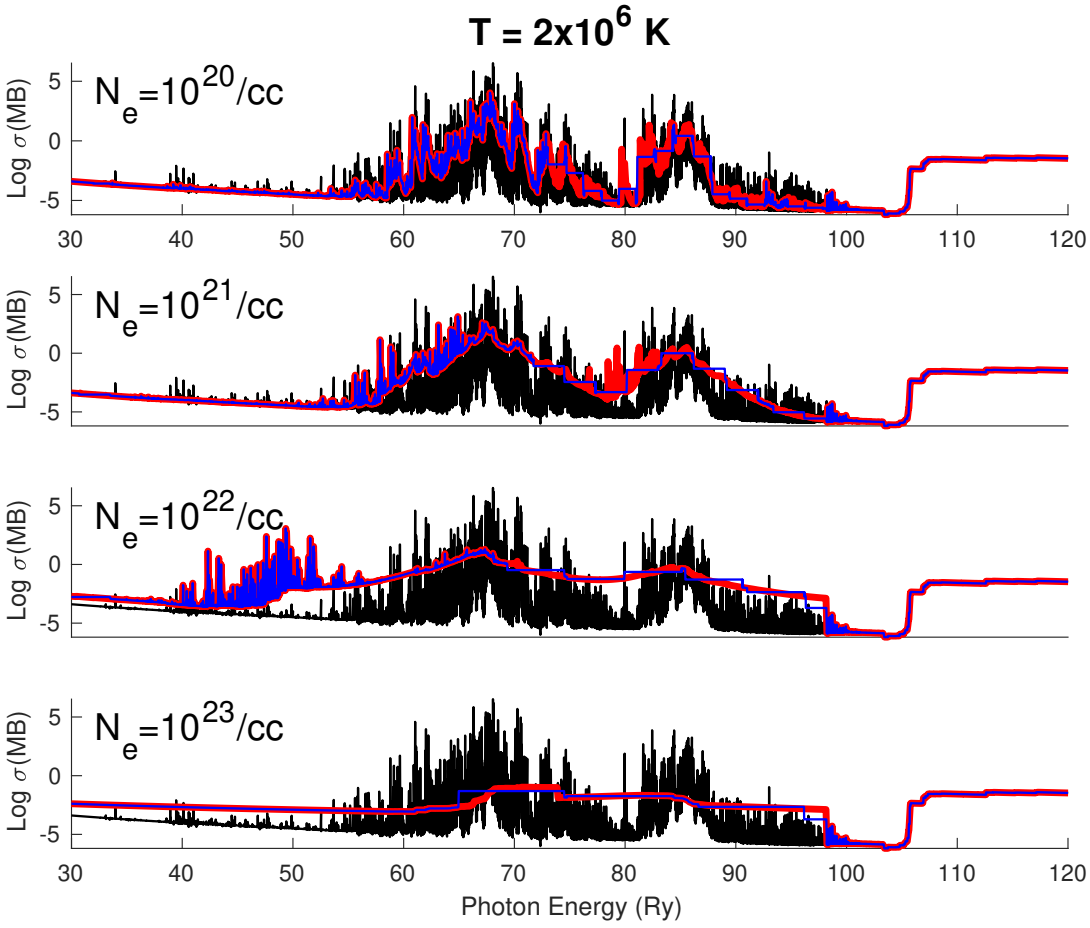

Fig. 1. Plasma broadened photoionization cross sections for $\hbar\omega$ + Fe xviii $\rightarrow e$ + Fe xix of the bound level $2s^2 2p^4\ [^3P^e_0]\ 5s(^2P_{1/2})$ (ionization energy 13.79 Ry), along the isotherm $T = 2 \times 10^6$K and electron densities $N_e = 10^{20,21,22,23}$/cc: black — unbroadened, red — broadened, blue — broadened with Stark ionization cut-off ν^*_s (Table 1). Rydberg series of AI resonance complexes with $\nu_i \leq 10$ belonging to 276 excited Fe XIX levels broaden and shift with increasing density, also resulting in continuum raising and threshold lowering. The two large features around 68 RY and 85 Ry are combinations of Seaton PEC and Rydberg series of resonances.

Table 1. Plasma parameters along isotherms 10^6K and 2×10^6K, and electron densities $N_e = 10^{20-23}$/cc for the (e + Fe XIX) $\longrightarrow$ Fe XVIII system w.r.t Fig. 1. Total AI resonance widths are shown at $\nu \approx 10$, with corresponding collisional widths Γ_c (10) and Stark width Γ_s (10). Effective quantum number ν_s^* refers to Stark ionization, and ν_D corresponds to the Debye radius. AI broadening widths are very weakly dependent on temperature and thermal Doppler widths are negligible in comparison with Γ_c and Γ_s .

T(K)	$N_e(cc)$	$\Gamma(\nu=10)$ Ry	$\Gamma_c(10)$ Ry	$\Gamma_s(10)$ Ry	ν_s^*	ν_D
10^6	10^{20}	5.98(-2)	7.56(-3)	5.23(-2)	14.6	43.2
10^6	10^{21}	3.18(-1)	7.56(-2)	2.43(-2)	10.8	24.3
10^6	10^{22}	1.88(0)	7.56(-1)	1.13(0)	7.93	13.7
10^6	10^{23}	1.28(1)	7.56(0)	5.22(0)	5.83	7.68
2×10^6	10^{20}	5.97(-2)	7.45(-3)	5.23(-2)	14.6	51.4
2×10^6	10^{21}	3.17(-1)	7.45(-2)	2.43(-1)	10.8	28.9
2×10^6	10^{22}	1.87(0)	7.45(-1)	1.13(0)	7.93	16.2
2×10^6	10^{23}	1.27(1)	7.45(0)	5.23(0)	5.83	9.13

Plasma effects on AI features Fig. 1 show a redward shift of low-n resonances and dissolution of high-n resonances. In addition, the background continuum is raised owing to redistribution of resonance strengths, which merge into one across high lying and overlapping thresholds. The shifts in AI resonance strengths, akin to line shifts but much more pronounced, is particularly important since cross sections are integrated over plasma particle distributions in order to obtain rates for atomic proceses. Also noteworthy is the height and extent of prominent resonances features dominated by Seaton PEC resonances. cross sections may range up to 10 orders magnitude in height and hundreds of eV in energy.

Table 1 gives plasma parameters corresponding to Fe XVIII at along two plasma isotherms and varying densities. The maximum width Γ_{10} corresponding to $\nu_i = 10$ in Eqs. 11,11,12 corresponding to the ν-mesh at which the unbroadened AI resonance profiles are delineated up to $\nu \leq 10$; an averaging procedure is employed up to $10 < \nu < \infty$ using quantum defect (QD) theory (viz. [6, 7]). $\Gamma_c(10)$ and $\Gamma_s(10)$ are the maximum collisional and Stark width components. The thermal Doppler width Γ_d is much smaller, as may be inferred from the fact that the total width Γ (10) $\approx \Gamma_c$ + Γ_s . However, in lower density plasmas $N_e < 10^{20}$/cc, Γ_d may be comparable to Γ_c or Γ_s.

In Table 1, the ν_s^* and ν_D are effective quantum numbers corresponding to Stark ionization cut-off and the Debye radius respectively. For HED plasmas with $N_e > 10^{23}$, one needs to examine if the bound orbitals are penetrated by the free electrons as the Debye length increases, and plasma screening effects may need to be considered. We therefore calculate the corresponding effective quantum number $\nu_D = \left[\frac{2}{5}\pi z^2 \lambda_D^2\right]^{1/4}$, where the Debye length $\lambda_D = (kT/8\pi N_e)^{1/2}$. It is seen in Table 1 that $\nu_D > \nu_s^*$ for all T, N_e considered, justifying neglect of plasma screening effects herein, but which may need to be accounted for at even higher densities.

AI broadening in a plasma environment affects each level cross section differently, and hence its contribution to opacities or rate equations for atomic processes in general. A critical (T,N_e) range can therefore be numerically ascertained where redistributed resonance phenomena would be significant and cross sections should be modified.

5. Conclusion

Atomic cross sections and rates in HED plasma sources at sufficiently high densities may be significantly affected by attenuation and broadening of AI resonant features. Precise evaluation of equation-of-state of the plasma determines the number of levels in predicting macroscopic properties such as

opacity and radiation transport. A computationally viable theoretical tratment taking account of plasma effects is reviewed. The method generalizes the description of AI phenomena of isolated Fano profiles in plasmas. Analogous to line shapes, atomic cross sections with resonant features become energy-temperature-density dependent, leading to broadening, shifting, and dissolving into myriad (e + ion) continua. However, unlike symmetric line profiles, the intrinsically asymmetric AI resonance shapes are attenuated over extended energy ranges. The predicted energy shifts of AI resonances as the plasma density increases should be experimentally verifiable. Redistribution of AI resonance strengths should manifest itself in rate coefficients for (e + ion) excitation, (e + ion) recombination, photoionization, opacities and radiation transport in HED plasma models, using temperature-dependent Maxwellian, Planck, or other particle distribution functions. The computational algorithm and a general-purpose program has been developed for large-scale computations.

Acknowledgments: I would like to thank Sultana Nahar for atomic data for Fe ions used in plasma AI broadening calculations.

Competing interests: The author declares there are no competing interests.

Data Availability Statement: There are no data associated with this review. However the papers [8, 9, 10, 11] refer to data from opacities calculations.

References

1. Fano U 1961 *Phys. Rev.* 124 1866
2. Rau A R P, 2004 *Phys. Scr.* 69 C10
3. Fano U and Rau A R P 1986 *Atomic Collisions and Spectra* (Academic Press, New York)
4. Burke P G 2011 *R-Matrix Theory of Atomic Collisions*, Springer
5. Lane A M and Thomas R G 1958 *Rev. Mod. Phys.* 30 257
6. The Opacity Project Team, 1995 *The Opacity Project*, Institute of Physics Publishing, Vol 1
7. Pradhan A K and Nahar S N 2011 *Atomic Astrophysics and Spectroscopy* Cambridge University Press
8. Pradhan A K, Nahar S N and Eissner W 2023 (to appear in *J. Phys. B*)
9. Nahar S N, Zhao L, Eissner W and Pradhan A K 2023 (to appear in *J. Phys. B*)
10. Pradhan A K 2023 (to appear in *J. Phys. B*)
11. Zhao L, Nahar S N and Pradhan A K 2023 (to appear in *J. Phys. B*)
12. Yu Y and Seaton M J *J. Phys. B* 20 6409
13. Mihalas D, Hummer D G and Däppen W 1988 *Astrophys. J.* 331, 815
14. Nahar S N and Pradhan A K 2016 *Phys. Rev. Lett.* 116 235003; Ibid. *Phys. Rev. Lett.* , 117, 249502
15. Hummer D G, Berrington K A, Eissner W, Pradhan A K, Saraph H E and Tully J A 1993 *Astron. Astrophys.* 279, 298
16. TOPbase URL: http://cdsweb.u-strasbg.fr/topbase/topbase.html
17. Inglis D R and Teller E 1939 *Astrophys. J.* 90 439
18. Dimitrijevic M S and Konjevic N 1987 *Astron. Astrophys.* 172 345
19. Nahar S N 2020 Atoms 8 68 (NORAD https://norad.astronomy.osu.edu/)